Oceanic and Atmospheric Anomalies Related to Tropical Instability Waves

Paulo S. Polito[1], John P. Ryan[2] and W. Timothy Liu[1]

Abstract.
Tropical instability waves (TIWs) are detected in remotely-sensed sea surface height (SSH), temperature (SST), and wind records of the eastern equatorial Pacific. The clearest TIW geophysical anomalies, evident at 3.5°N, are isolated by 2D filtering. Relationships between anomalies are examined by cross-correlation and phase offsets. The 72% correlation and 90° phase lag between SSH and SST indicate that TIW SST anomalies are mostly due to advection of the meridional temperature gradient by TIW geostrophic currents and emphasize the importance of SSH measurements. Meridional wind anomalies are well correlated (70%) and have a 90° phase lag with SSH. This supports that in the spectral band of TIWs the sea surface roughness measured by the scatterometer is significantly influenced by ocean currents. This causes wind anomalies to have similar speed but opposite direction of TIW surface currents. Ekman pumping (EkP) anomalies are well correlated with both SSH (62%) and SST(62%). Scaling and phase relationships support that EkP anomalies are an effect rather than a cause of the oceanic anomalies.

Introduction

Equatorial Pacific TIWs have been observed and modeled for more than two decades (*Legeckis* [1977]; *Cox* [1980]; *Halpern et al.* [1988]; *Yu et al.* [1995]; *Qiao and Weisberg* [1998]). TIWs are Rossby or Rossby-gravity waves whose phase always propagates westward and whose group velocity can be either westward or eastward. The waves are generated by barotropic instability and are seasonally and interannually modulated by variations in the system of currents that sustains them.

TIW horizontal phase propagation is mainly zonal with phase speeds (c_p), wavelengths (λ) and periods (P) on the order of -35 km day^{-1}, 1000 km and 30 days. These attributes are based on observational and theoretical results that can vary by more than a factor of two (*Qiao and Weisberg* [1995]), depending on latitude, instrumentation, and time, among other factors.

[1]Jet Propulsion Laboratory,California Institute of Technology, Pasadena, California
[2]Monterey Bay Aquarium Research Institute, Moss Landing, California

Theory

We present basic theory for phase and scaling arguments essential to interpretation of anomaly relationships.

TIWs are evident as westward propagating anomalies in SSH (η) and SST (SST′). η are mostly caused by variations in the density of the water column, dominated by temperature (thermosteric) fluctuations:

$$\eta = \alpha \int_h^0 T(z)\, dz, \qquad (1)$$

where α is the thermal expansion coefficient, $T(z)$ the temperature anomaly profile and h a depth below the main thermocline. In Equation 1, a 1°C anomaly extending to 300 m results in a η of 0.1 m. If the temperature anomaly extends to depth h, η and SST′ should be in phase.

Strong meridional current fluctuations are associated with TIWs. Owing to equatorial upwelling, the poleward temperature gradient is positive and relatively strong where TIWs develop. SST′ due to advection of the meridional SST gradient ($\frac{\partial SST}{\partial y}$) by a meridional geostrophic current anomaly (v_o') acting for a period P

are:

$$SST' = v'_o \frac{\partial SST}{\partial y} P, \text{ with } v'_o = \frac{g}{f} \frac{\partial \eta}{\partial x}, \qquad (2)$$

where g is gravity, f the Coriolis parameter and x the zonal dimension. Heat and mass exchange are neglected. In Equation 2, a 0.2 m s^{-1} v'_o acting for 15 days in the presence of a meridional SST gradient of 5×10^{-6} °C m^{-1} results in a SST′ of 1.5 °C. If forced by TIW meridional currents, SST′ should lag η by 90°.

Subsurface density fluctuations induce SSH fluctuations which are dependent upon the stratification. EkP anomalies (EkP′) cause density fluctuations in the Ekman layer, and thus influence η. The vertical velocity at the base of the Ekman layer is given by the EkP equation, and the vertical velocity of the surface ($\frac{\partial \eta}{\partial t}$) induced by wind forcing is given by EkP′ scaled by the stratification:

$$\frac{\partial \eta}{\partial t} = -\frac{\nabla_k \times \vec{\tau}}{\Delta \rho f}, \qquad (3)$$

where $\Delta\rho$ is the density difference between the layers above and below the base of the Ekman layer, and $\nabla_k \times \vec{\tau}$ is the vertical component of the wind stress curl. The wind stress curl is in phase with the vertical velocity and thus at 90° with its integral, η (assuming sinusoidal variations). With thermal stratification, Ekman upwelling can result in SST cooling. In Equation 3, a wind anomaly of 3 m s^{-1} over $\frac{1}{2}\lambda$ of a TIW would force vertical displacement of $\sim$ 10 m in 15 days. In this region, the thermal stratification is such that a 10 m displacement would result in a SST′ of $\sim$ 0.5 °C.

Data Sets and Methods

The satellite data sets used in this study are WOCE TOPEX/POSEIDON SSH, daily 9-km AVHRR Pathfinder SST, and daily NASA Scatterometer (NSCAT) 0.5° Level 3 winds. The period examined coincides with the NSCAT period, September 1996 through May 1997. The spatial domain extends between the date line and 100° W, 10.5°S and 10.5°N. The SSH data were acquired bin-averaged at 0.5° × 0.5° × 10.0 days. Daily SST and wind fields were averaged into 7-day, 2° latitude bins at the zonal resolution of the data. For computing EkP, wind stress was calculated according to *Large and Pond* [1981]. All data sets were interpolated *via* bicubic gridding to a common 0.5° × 7-day zonal-temporal grid.

Anomalies were computed for all variables by removing the temporal mean. Anomaly time series were then band-pass filtered using the same series of 2D (zonal-temporal) finite impulse response filters (*Polito and Cornillon* [1997]) which yield nearly zero phase distortion and a smooth transition between the stop and pass bands. The strength of the TIW signal in each variable is estimated by the amount of total variance explained by the filtered signal (σ). For each pair of variables the zonal-temporal cross-correlation matrix was calculated. A sinusoidal surface was least-squares fit to the correlation to obtain the maximum correlation (C_{max}) within one λ and P of the origin, and the average phase difference ($\Delta\Phi$). Because of the coarse resolution of the data in relation to the wave period, $\Delta\Phi$ are estimated only to the nearest 90° increment.

Results and Discussion

TIW signals are most clearly evident in the 2° latitude bands centered at 1.5°N and 3.5°N, between 160°W and 120°W and October/96 through January/97. Outside this band the fractional variance of the filtered SST′ signal is <10%, and its correlation with η is <50%. Because the amount of variance explained by the filtered signals was greatest at 3.5°N, we present results from this latitude band (Figure 1). The TIW signals are evident in zonal-temporal plots as diagonally-oriented bands of positive and negative anomalies whose orientation indicates westward phase propagation. TIW anomalies are evident in the unfiltered data, together with strong large scale signals that are removed by the 2D band-pass filter. From filtered anomalies, the estimates of $c_p \sim 37$ km day^{-1}, $P \sim 30$ days, and $\lambda \sim 1100$ km are in agreement with previous estimates for TIWs (*Qiao and Weisberg* [1995]). Anomaly statistics are summarized in Table 1.

The high correlation and quadrature of phase between η and SST′ (Table 1) have two important interpretations. First, they indicate that TIW SST′ are not in phase with upper layer thermosteric anomalies (Equation 1). Second, they suggest that advection of the meridional temperature gradient by TIW geostrophic currents causes SST′ (Equation 2). This is illustrated in Figure 2: northward currents associated with the positive zonal η slopes of TIWs advect cold SST northward, while southward currents associated with negative zonal η slopes advect warm SST southward. This interpretation is consistent with high resolution mapping of circulation and SST over a TIW (*Flament et al.* [1996]).

Meridional wind anomalies (v') also show a strong, clear TIW signal (Figure 1). v' are highly correlated with both η and SST′ and are in quadrature with η (Table 1) thus in opposition of phase with TIW

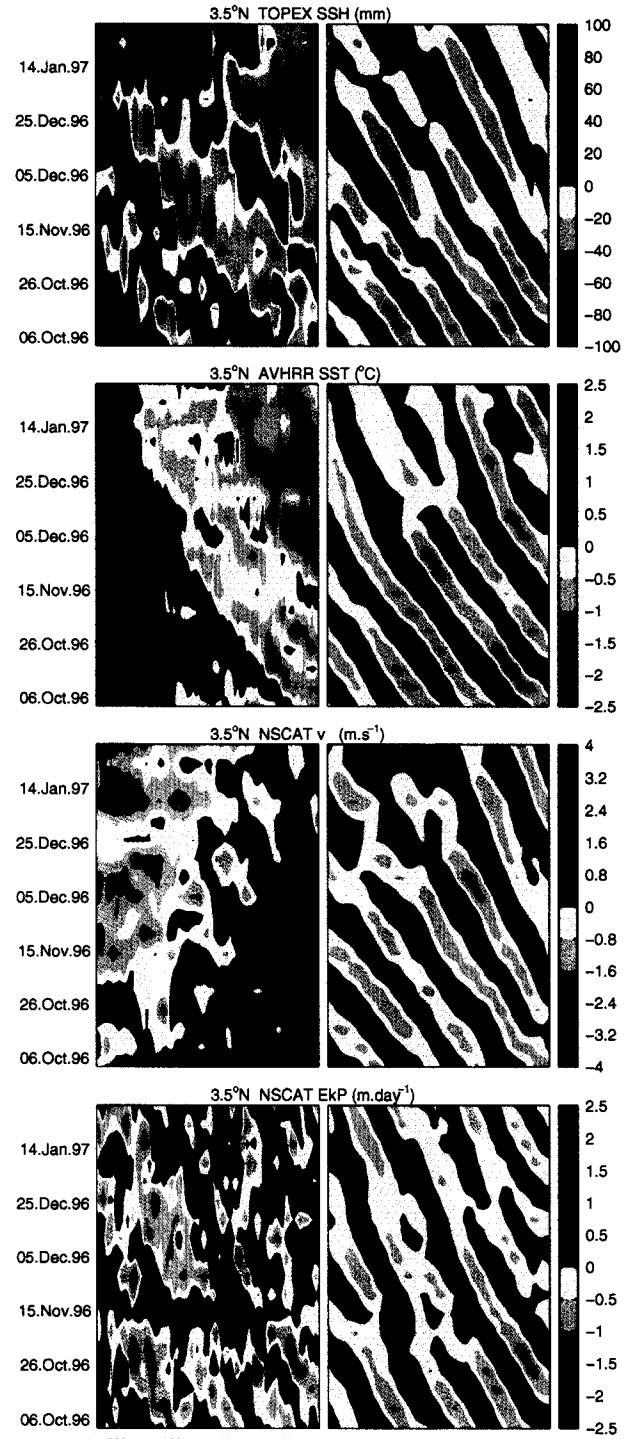

Figure 1. Zonal-temporal diagrams of unfiltered (left) and filtered (right) η, SST$'$, v' and EkP$'$.

Table 1. Summary of the results. Positive $\Delta\Phi$ indicates that the the first parameter leads the second.

parameter	σ	parameters	$\Delta\Phi$	C_{max}
η	29%	η,SST$'$	90°	72%
SST$'$	29%	η,v'	90°	70%
v'	26%	η,EkP$'$	0°	62%
EkP$'$	39%	SST$'$,v'	0°	65%
		SST$'$,EkP$'$	−90°	62%
		v',EkP$'$	−90°	51%

geostrophic surface currents. A plausible hypothesis for a relationship between η and v' in this spectral band is that ocean currents affect scatterometer wind retrievals (P. Cornillon 1999, personal communication). The scatterometer measures surface roughness, dependent upon the relative motion between atmosphere and ocean. We propose that scatterometer winds over TIWs are biased by enhanced surface roughness caused by surface currents. This bias has similar magnitude and opposite direction of TIW surface currents (Figure 2).

The TIW signal is pronounced in EkP$'$(Figure 1) that are strongly correlated with both η and SST$'$ (Table 1). η and EkP$'$ are in phase. Because the expected phase lag for EkP$'$ forcing η is 90° (Equation 3), TIW η could not be forced by EkP$'$. Based on correlation and phase relationships, we have argued that TIW SST$'$ are predominantly forced by meridional geostrophic current anomalies (Figure 2). Although EkP$'$ can force SST$'$, this relationship is not supported. First, EkP$'$ leads SST$'$ by 90° (Table 1). For EkP$'$ forcing of SST$'$, SST$'$ should lead EkP$'$ by 90°. Second, considering the relatively weak thermal stratification of the upper 10 m, SST cooling by Ekman upwelling would be $\sim$ 0.5 °C, significantly less than the observed SST$'$ (Figure 1). Thus, although EkP$'$ is strongly correlated with both η and SST$'$, the aggregate results support that TIW EkP$'$ do not force TIW η or SST$'$.

The EkP$'$ results are consistent with the hypothesis of winds biased by ocean currents (Figure 2). East (west) of a positive η, meridional winds would have a northward (southward) anomaly. This would appear as a wind stress curl anomaly in phase with η, as observed. EkP$'$ due to surface ocean currents are analogous to inverted Ekman pumping resulting from bottom friction. Although these results are internally consistent, we have not yet examined the role of thermodynamic forcing. The observed EkP$'$ may result from a combination of dynamic and thermodynamic forcing.

There is an important distinction between the influ-

ence of ocean currents on scatterometer wind velocity estimates and EkP derived from scatterometer winds. The results presented here support that wind velocity bias is caused by scatterometer detection of enhanced stress at the air-sea interface due to ocean currents. Although wind velocities are biased, the enhanced stress causing the bias is real, and thus so are the EkP′. This real dynamical effect may have important biological implications. Convergence and divergence that develop with TIWs affect biological distributions and processes (*Yoder et al.* [1994]; *Flament et al.* [1996]; *Chavez et al.* [1999]). TIW EkP′ may force variation in vertical nutrient flux in this biogeochemically important upwelling system. Thus we state not only caution regarding bias in scatterometer wind velocities, but also motivation to understand dynamical and biological effects of air-sea stress anomalies associated with TIWs, and the role of thermodynamic forcing in this air-sea coupling.

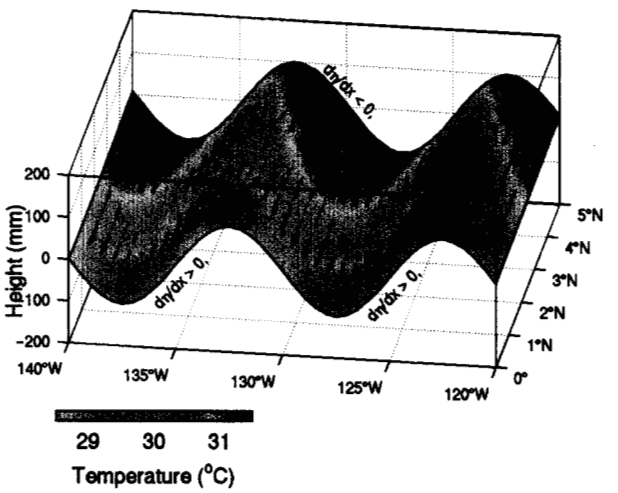

Figure 2. Scatterometer winds (red arrows) mirror the sea surface currents (black arrows), are in phase with the SST (colors) and in quadrature with η (sinusoid).

Acknowledgments. The authors are indebted to their host institutions for support of this study. P. Polito was jointly supported by the Physical Oceanography and Earth Observing System Interdisciplinary Sciences Programs of NASA. We thank the Physical Oceanography Distributed Active Archive Center at NASA Jet Propulsion Laboratory for provision of all satellite data sets used in this study. Acquisition of the NSCAT Level 3 data were facilitated by the Distributed Oceanographic Data System (http://www.unidata.ucar.edu/packages/dods).

References

Chavez, F. P., P. G. Strutton, G. E. Friedrich, R. A. Feely, G. Feldman, D. Folay and M. J. McPhaden, Biological and chemical response of the equatorial Pacific Ocean to the 1997-98 El Niño, *Science*, *in press*, 1999.

Cox, M. D., Generation and propagation of 30-day waves in a numerical model of the Pacific, *J. Phys. Oceanogr.*, *10*, 1168–1186, 1980.

Flament, P. J., S. C. Kennan, R. A. Knox, P. P. Niiler and R. L. Bernstein, The three-dimensional structure of an upper ocean vortex in the tropical Pacific Ocean, *Nature*, *383*, 610–613, 1996.

Halpern, D., R. A. Knox, and D. S. Luther, Observations of 20-day period meridional current oscillations in the upper ocean along the pacific equator, *J. Phys. Oceanogr.*, *18*, 1514–1534, 1988.

Large, W. G. and S. Pond, Open ocean momentum measurements in moderate to strong winds. *J. Phys. Oceanogr.*, *11*, 324–336, 1981.

Legeckis, R., Long waves in the eastern equatorial Pacific ocean: a view from a geostationary sattelite, *Science*, *197*, 1179–1181, 1977.

Polito, P. S., and P. Cornillon, Long baroclinic Rossby waves detected by TOPEX/POSEIDON, *J. Geophys. Res.*, *102*, 3215–3235, 1997.

Qiao, L., and R. H. Weisberg, Tropical instability wave kinematics: observations from the tropical instability wave experiment (TIWE), *J. Phys. Oceanogr.*, *100*, 8677–8693, 1995.

Qiao, L., and R. H. Weisberg, Tropical instability wave energetics: observations from the tropical instability wave experiment, *J. Phys. Oceanogr.*, *28*, 345–360, 1998.

Yoder, J. A., S. G. Ackleson, R. T. Barber, P. Flament and W. M. Balch, *Nature*, *371*, 689–692, 1994.

Yu, Z., J. P. McCreary, and J. A. Proehl, Energetics of tropical instability waves, *J. Phys. Oceanogr.*, *25*, 2997–3007, 1995.

P. S. Polito and W. T. Liu, Jet Propulsion Laboratory, California Institute of Technology, 4800 Oak Grove Dr., MS 300-323, Pasadena CA 91109. (e-mail: polito@pacific.jpl.nasa.gov; liu@pacific.jpl.nasa.gov)

J. P. Ryan, Monterey Bay Aquarium Research Institute, 7700 Sandholdt Road, Moss Landing, CA 95039. (e-mail: ryjo@mbari.org)